Pharm Res (2011) 28:720–730
DOI 10.1007/s11095-010-0353-x

RESEARCH PAPER

In Vivo Anti-Tumor Effect of Expressing p14ARF-TAT Using a FGF2-Targeted Cationic Lipid Vector

Guoqin Niu • Wouter H. P. Driessen • Sean M. Sullivan • Jeffrey A. Hughes

Received: 11 August 2010 / Accepted: 14 December 2010 / Published online: 19 January 2011

ABSTRACT

Purpose To develop an efficient and safe strategy to introduce a therapeutic gene into target cells *in vivo* for cancer therapy. The overall efficiency is based on proper selection of the delivery vector and expressed protein.

Methods A plasmid coding for a specific cytotoxic fusion peptide, p14ARF-TAT, was evaluated in a xenograft mouse tumor model. The expressed peptide consisted of three domains, a secretory signal, a membrane permeability segment and a cytotoxic fragment. Gene expression was verified in U87-MG cells by Western blot and cytotoxicity confirmed with CyQuant assay. To improve the delivery, a FGF2 targeting peptide, MQLPLATC, was incorporated into the vector, which was evaluated using a luciferase-expressing plasmid.

Results The luciferase activity *in vitro* was two-fold higher with the targeted formulations, and cytotoxicity was three-fold higher with expression of the p14ARF-TAT protein. A murine xenograph model of human glioma (U87-MG cells) tumors was used to address *in vivo* activity. FGF2-targeted lipoplexes demonstrated increased tumor volume reduction as compared to non-targeted formulations. RT-PCR and Western blot of tumor homogenizes indicated p14ARF-TAT expression in tumors along with other tissues.

Conclusion p14ARF-TAT was cytotoxic and is a promising approach when combined with an efficient targeting.

KEY WORDS anti-tumor effect · cationic liposome · fibroblast growth factor (FGF2) · fusion cytotoxic gene · lipid-based gene delivery

INTRODUCTION

Gene therapy is an important strategy to treat inherited or acquired diseases, such as cancer (1). A successful gene therapy approach contains three critical elements: the functional gene, effective delivery vector and suitable delivery route. Currently, viral vectors are the main vehicles in several clinical applications due to highly efficient gene delivery. However, immunogenicity, non-specificity and inherent risks of complications (2) make non-viral vectors also attractive. Among non-viral vectors, cationic lipids have been widely investigated in preclinical and clinical trials because their *in vitro* transfection efficiency is comparable to that of viral vectors, although their use could be associated with non-specificity and cytotoxicity (3). The non-specificity can be addressed by incorporating a targeting ligand.

Among the tumor-selective targeting ligands, basic fibroblast growth factor (bFGF or FGF2) has received considerable attention. FGF2 receptor is over-expressed in many cancer cell lines (4,5), including the U87-MG glioma

Electronic Supplementary Material The online version of this article (doi:10.1007/s11095-010-0353-x) contains supplementary material, which is available to authorized users.

G. Niu • W. H. P. Driessen • J. A. Hughes
Department of Pharmaceutics, College of Pharmacy
University of Florida
Gainesville, Florida 32610, USA

W. H. P. Driessen
M. D. Anderson Cancer Center
1515 Holcombe Blvd.
Houston, Texas 77030, USA

S. M. Sullivan
Vical Incorporated
10390 Pacific Center Court
San Diego, California 92121, USA

J. A. Hughes (✉)
340 Kingsland Street
Nutley, New Jersey 07110-1199, USA
e-mail: hughes@cop.ufl.edu

cell line (6–10); also, the FGF receptor is up-regulated on endothelial cells proliferating during angiogenesis (5,11). FGF2 has complex biological properties (12), is mitogenic, shows limited stability in serum, and has a tendency to bind heparins and other anionic proteins in the plasma. In this study, a short peptide MQLPLATC was used, which is demonstrated to bind to FGF receptor without receptor activation (13) but can result in targeted gene expression (14).

Effective gene therapy for cancer requires a majority of tumor cells be impacted by gene transfer, directly or indirectly. Current vectors are limited in achieving this goal. For this reason, methods increasing transgene spread to adjacent cells are beneficial. One approach is the use of transfected cells as a bioreactor. In order for the bioreactor approach to be effective, the expressed transgene requires particular properties. With this in mind, we crafted a plasmid vector encoding a gene with three domains: 1) a secretory signal domain (15), with the sequence of MLGPCMLLLLLLLGLRLQLSLG, based on secretory alkaline phosphatase; 2) a membrane permeability domain (16–18), with the sequence of YGRKKRRQRRR, based on HIV TAT; and 3) a cytotoxic domain, with the sequence of MVRRFLVTLRIRRA, p14ARF which can induce cellular apoptosis via the p14ARF-mdm2-P53 pathway (19–21).

We (22) have previously reported the *in vitro* activity of synthetic peptides modeling the composite of the gene product, in which two membrane translocation domains (PTDs) for the delivery of mdm-2 peptide binding domain were compared. A summary of the findings indicated a peptide composed of an HIV Tat sequence and mdm-2 binding domain sequence were optimal for cytotoxicity *in vitro*.

In this study, a p14ARF-TAT (pARF) expression plasmid was formulated into a cationic lipoplex and verified for gene expression, cytotoxicity and cellular apoptosis. FGF2-targeted cationic liposomes were also evaluated for targeting. The *in vivo* anti-tumor effect of pARF gene was evaluated in nude/nude mice bearing human glioblastoma U87-MG tumors by targeted and non-targeted systems.

MATERIALS AND METHODS

1-(N4-spermine)-2, 3-dilaurylglycerol carbamate (Genzyme lipid 89) was provided by Genzyme, Cambridge, MA). 1,2-distearoyl-*sn*-glycero-3-phosphoethanolamine-N-[PDP(polyethylene glycol)-2000 (PDP-PEG2000-DSPE), Lym-X-Sorb (lysophosphatidylcholine : glycerol monooleate : oleic acid = 1:4:2), 1,2-distearoyl-*sn*-glycero-3-phosphoethanolamine-N-[methoxy (polyethylene glycol)-2000] (MPEG2000-DSPE) and other lipids were kindly provided by Avanti Polar Lipids, Inc. AL. FGF2 peptide (MQLPLATC) was synthesized by ICBR Proteomics Lab, University of Florida). CyQUANT Cell Proliferation Assay Kit was purchased from Molecular Probes, Inc., Eugene, OR. U87-MG cells were purchased from American Type Culture Collection. Halt Protease Inhibitor Cocktail was from Pierce Biotechnology, Rockford, IL.

Plasmid Construction and Preparation

The expression cassette for pARF was composed of a CMV promoter (23), a consensus intron exon, an alkaline phosphatase signal sequence (15), HIV-Tat (16–18), p14ARF (19), influenza hemaglutinin epitope and human growth hormone poly A, which was constructed using a kanamycin resistance backbone (Fig. 1). The HIV Tat peptide corresponded to amino acids 47 to 56 (YGRKKRRQRR) of Tat (24), to which AGGG was added to the N-terminus (17). The DNA sequence for the mdm-2 binding domain corresponded to amino acids 42 to 55 from p14ARF, (MVRRFLVTLRIRRA). The secreted alkaline phosphatase signal was (MLGPCMLLLLLLLGLRLQLSLG). The HA epitope was 9 amino acid sequence from the influenza hemmaglutinin envelope protein (YPYDVPDYA) to aid in detection of the expressed protein. The complete sequence is provided in the Supplementary Material.

The plasmid was produced in DH5 alpha *Escherichia coli* with kanamycin and concentrated to a final concentration of 2 mg/ml. The plasmid purity was confirmed by agarose gel electrophoresis, and DNA concentration was measured by UV absorbance at 260 nm. The percentage of supercoiled DNA and OD260/280 ratios of these plasmid preparations were in the range of 70–95% and 1.8–1.9, respectively.

Synthesis of FGF2-PEG-DSPE

PDP-PEG2000-DSPE (1,2-distearoyl-*sn*-glycero-3-phosphoethanolamine-N-[PDP(polyethylene glycol)-2000), 40 µl (10 mg/ml, 0.134 µmol) in chloroform, was dried using argon, and the residual solvent was removed by placing the tube in vacuum desiccators for 2 h. The lipid film was hydrated with 122 µl Hepes buffered saline (HBS, 7.5 mmol/l Hepes, 150 mmol/l NaCl, pH7.4) and mixed with 28 µl FGF2 peptide (6.2 mg/ml, 0.198 µmol), then shaken 4 h at room temperature (25–27). The resulting solution was dialyzed overnight against 4.0 L of pure water using a Slide-A-Lyzer® dialysis cassette with a cut-off size of 2000 MW (Pierce, Rockford, IL), and lyophilized for 48 h using FreeZone 6 freeze dry systems (Labconco Corporation, Kansas City, MO). The FGF2-PEG-DSPE was characterized by ^{1}H-Nuclear Magnetic Resonance (^{1}H-NMR). The sample was dissolved in $H_2O/D_2O/CD_3CN$ (80:8:12, V/V), and the ^{1}H-NMR spectroscopic data were carried out with Bruker Avance 500 Console, Magnex 11.75T/54 mm Magnet Advanced Magnetic Resonance Imaging and Spectroscopy (McKnight Brain Institute, University of Florida).

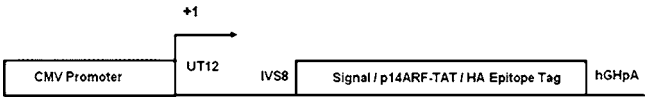

Fig. 1 pARF gene expression cassette +1 means the start point of the transcription. UT12 is the modified 5′ untranslated region (UTR) from the CMV immediate early gene and IVS 8 [intron-8 polythymidine sequence] is a synthetic intron. Signal refers to the signal sequence for secreted alkaline phosphatase. hGHpA refers to the human growth hormone polyadenylation sequence.

Preparation of Lipoplex (28)

The lipid-based transfection reagent (Genzyme lipid 89: Lym-X-Sorb:Vitamin E 10:89:1, GLL, structure shown in Fig. 2) was prepared by mixing 40 µl of Genzyme lipid 89 (25 mg/ml in chloroform or 0.038 µmol/µl) (29), 37.5 µl Lym-X-Sorb (138 mg/ml in chloroform or 0.365 µmol/µl, LXS), and 11 µl Vitamin E (5.905 mg/ml or 0.0137 µmol/µl) (Sigma, St. Louis, MO) in a clean reagent tube. The solvent chloroform was evaporated by Argon and then further dried in a vacuum desiccator for 4 h. The dry film was hydrated with HBS under an aseptic condition, vortexed briefly and bath sonicated (5 min) until a transparent solution was obtained. Plasmid was mixed with GLL and incubated for 15 min at room temperature before administration. For pegylated (MGLL) or FGF2-targeted (FGLL) lipoplex, calculated MPEG2000-DSPE or FGF2-PEG-DSPE was added to the plasmid-GLL complex and incubated 1 h at 37°C (30). The mole ratio of GL89 to DNA used was 2:1 (N/P ratio was 4:1, weight ratio was 4:1). The resulting plasmid-GLL complex contains 50 µg plasmid DNA per 150 µl for the *in vivo* test.

Particle Size Measurement

Particle size distribution and mean diameter of the lipid mixture and plasmid/lipid mixture complex were determined by quasi-elastic light scattering using a NICOMP 380 Submicron Particle Sizer (Santa Barbara, CA, USA) equipped with 5 mW helium-neon laser at 632.4 nm and a temperature-controlled cell holder as described previously (31). The mean particle diameter, d_h, was obtained from Stokes-Einstein relation using the measured diffusion of particles in solution ($\eta = 0.933$, $T = 23°C$, $n = 1.33$). Data were analyzed in terms of volume-weighted distributions. Each reported experimental result is the average of at least three d_h values obtained from analysis of the autocorrelation function accumulated for at least 20 min.

Zeta Potential Measurement

Particle surface charge analysis was performed using a ZetaPlus Zeta Potential Analyzer instrument (Brookhaven Instruments, Holtsville, NY). In order to have the signal intensity within the limits required by the instrument and also to maintain the size range, the lipid mixture was hydrated with pH 7.4, 10 mM Hepes buffer, 0.15 M NaCl. Then, samples were diluted eight times with distilled water. The zeta-potential of each sample was determined from five to eight independent measurements.

Cell Culture

U87-MG cells were purchased from American Type Culture Collection and cultivated in Dulbecco's modified essential medium (DMEM, Sigma), supplemented with 10% fetal bovine serum and 1% penicillin–streptomycin. The U87-MG cells were incubated at 37°C in humidified environment of 5% CO_2. The medium was replenished every other day, and cells were sub-cultured after reaching confluence.

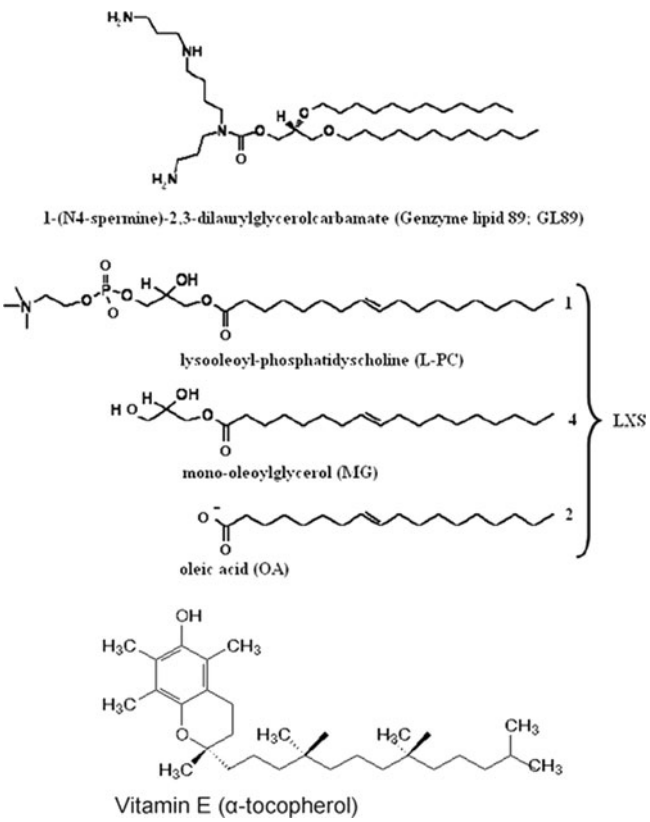

Fig. 2 Structure of the lipoplex components.

Transfections

U87-MG cells were seeded in 24-well plate at 50%–60% confluency the day before the transfection. pARF plasmid was complexed with GLL at GL89/DNA =2:1 (mole ratio). The plasmid was mixed with GLL and diluted to the concentration of 2.5 μg/ml DNA with DMEM, and 0.5 μg/0.2 ml/well was used for transfection. After 4–6 h incubation at 37°C, 5% CO_2 humidified air, the serum-free media was changed with complete media. After 48 h incubation, the cells were washed with cold PBS and stored at −80°C until assaying with Cyquant Assay. To the comparison of transfection in serum-free and with-serum media, the lipoplex was transfected in serum-free or with-serum media containing DMEM and 1% penicillin–streptomycin.

For the Western blot detection of pARF expression, cells were placed on a six-well plate at 70–80% confluency the day before the transfection. pARF plasmid was complexed with GLL at GL89/DNA =2:1 (mole ratio), and 4 μg/0.8 ml plasmid was added to the cells and incubated 4 h in 37°C, 5% CO_2 humidified air. A non-coding plasmid vector pVC1157 (pE) was also transfected as a control. Serum-free media was changed with complete media. After 48 h, the cells were harvested with RIPA buffer, containing 1% Halt Protease Inhibitor Cocktail and 1 mM PMSF, stored at −20°C until Western blot was performed.

In Vivo Tumor Treatments

In all the *in vivo* experiments, 2×10^6 tumor cells (U87-MG) suspended in 100 μl sterile PBS were injected into the right dorsal flank of female nude/nude mouse. Tumor size was measured every day. The well-defined tumor mass was measured by averaging the diameters using a Digital Caliper. Tumor measurements were recorded every day, and tumor volumes were calculated by using the formula V (mm^3) = $a*b*c/2$, where a is the largest dimension, b is the perpendicular diameter, and c is the height (32).

Antitumor efficacy data are presented as cumulative tumor volumes for all animals in each group. Tumors were weighed when the animals were sacrificed.

For the treatment experiment, subcutaneous U87-MG tumor-bearing nude mice were divided into four groups of six mice per group. Group 1 received PBS, group 2 received pE -GLL complex (50 μg DNA/dose), group 3 received pARF-GLL complex (50 μg DNA/dose), and group 4 was injected with pARF-FGLL (50 μg DNA/dose). Animals were injected at the fourth and eleventh day post-tumor-cells-implantation via tail vein injection.

The statistical significance of multi-groups was determined by using one-way ANOVA analysis with multi-comparison (Tukey HSD test).

In Vivo Transfection Efficiency in Subcutaneous Tumors

Nude mice were injected with U87-MG tumor cells (2×10^6/100 μl of PBS) subcutaneously on the right flank. When the tumors reached 25–40 mm^3, a single dose of pARF-GLL complex (100 μg pARF/200 μl) was injected via tail vein. Twenty-four hours after injection, mice were euthanized by CO_2 inhalation, and tumors were removed and snap frozen using liquid nitrogen for RT-PCR identification and Western blot analysis for pARF expression. For TUNEL (TdT-mediated dUTP nick end labeling) staining (*In Situ* Cell Death Detection Kit, Fluorescein; Roche Diagnostics, Indianapolis, IN), the tumors were removed and immersed in freshly made 4% paraformaldehyde in PBS and then transferred into 30% sucrose for cryoprotection and frozen at −80°C.

Identification of pARF mRNA

Total RNA was extracted from the tumors using TRI® Reagent (Sigma, St. Louis, MO, USA). QIAGEN® OneStep RT-PCR kit (QIAGEN GmbH, Germany) was used for the identification of pARF mRNA. The RT-PCR was done with a Mastercycler gradient (Eppendorf North America, Westbury, NY) according to the manual of the kit. The specific primers were 5′-CCTTCCCCTGCTATTCTGCT-3′ (forward) and 5′-GCCCCTTGCTCCATACCAC-3′ (reverse). The expected complementary DNA had 522 bp. The thermal cycler conditions were 50°C 30 min for reverse transcription, 95°C 15 min for initial PCR activation step, and with three-step cycling: denaturation 94°C 1 min, annealing 60°C 1 min and extension 72°C 1 min, 40 cycles, and final extension 72°C 10 min, 4°C in the end. Amplified fragment was separated by 2.0% agarose gel electrophoresis and visualized with ethidium bromide. Control reactions were kept on ice and placed in the thermal cycler only after it has reached 95°C for polymerase activation step (before cycling).

Table 1 Size and Zeta Potential of Plain and Targeted Lipoplex (mean ± SD, $n=3$)

	GLL	FGLL	DNA-GLL	DNA-FGLL
SIZE (nm)	107.1 ± 14.6	114.1 ± 11.0	289.3 ± 34.8	232.6 ± 29.0
Zeta Potential (mV)	34.48 ± 2.55	32.11 ± 1.96	28.07 ± 1.59	25.08 ± 2.67

Western Blot Analysis

For tumor lysis, the lysis buffer contains 1× RIPA buffer (Cell Signaling Technology, Danvers, MA), 1 mM PMSF (phenylmethylsulphonyl fluoride, Alexis Biochemicals, San Diego, CA) and 1% Halt™ Protease Inhibitor Single-use Cocktail (Pierce, Rockford, IL). The tumors were weighed and put into a 2 ml tube, and 1 ml lysis buffer/0.1 g tumor was added, and then the tumors were cut and homogenized using Power Gen 125 (Fisher Scientific, Pittsburgh, PA), lyzed 30 min on ice, and centrifuged 13,000 rpm for 10 min at 4°C. The supernatant was ready for Western blot analysis. The protein concentration was measured by BCA protein assay kit (Pierce, Rockford, IL).

For Western blot detection of pARF product, tumor extracts (75 μg/lane) were resolved on a 16.5% Tris-Tricine/SDS–polyacrylamide gel electrophoresis (Bio-Rad, Hercules, CA), transferred to 0.2 μm PVDF membrane (Invitrgen, Carlsbad, CA) at 100 volts for 1 h, and probed with anti-HA-tag mouse monoclonal antibody (1:1000 dilution in 5% fat free milk, Cell Signaling Technology, Danvers, MA). Anti-mouse secondary antibodies labeled with horseradish peroxidase (1:5000 dilution in 5% fat free milk, Chemicon International, Temecula, CA) were used.

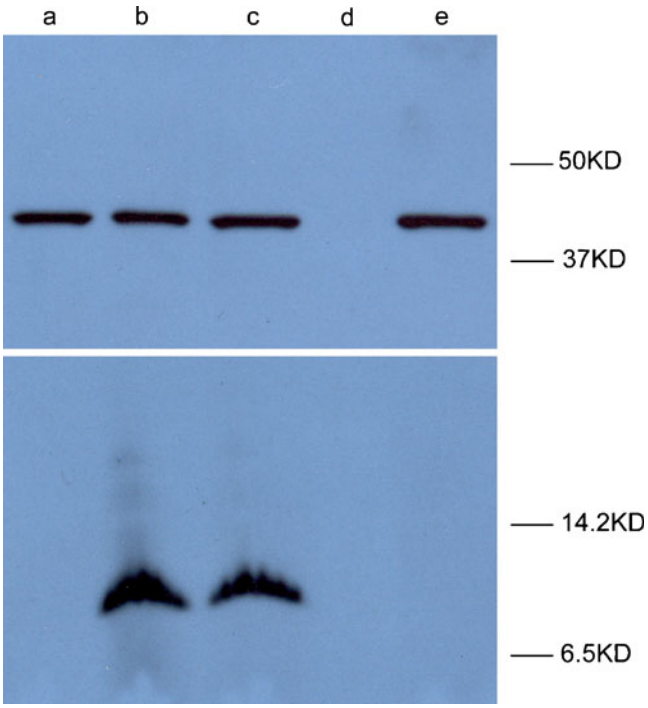

Fig. 3 Western blot detection of pARF expression U87-MG cells were transfected with pARF or *empty vector* pE using GLL. Lane a—non-treated cells; Lane b—pARF transfected by FGLL, 3 μg/well on 6-well plate; Lane c—pARF transfected by GLL, 3 μg/well on 6-well plate; Lane d—color marker ultra-low range (Sigma C6210) and Precision Plus Protein Kaleidoscope standards for beta-actin detection; Lane e—pE-transfected cells.

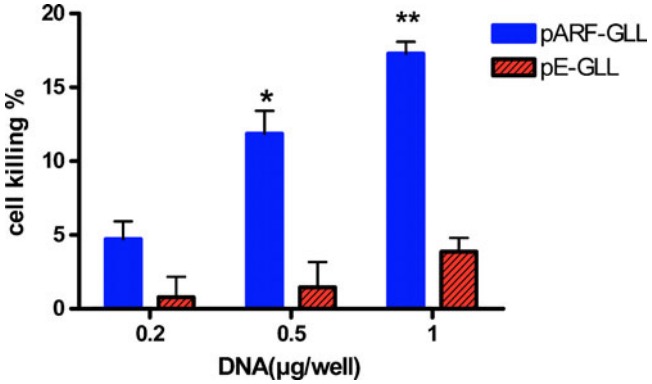

Fig. 4 Cytotoxicity of pARF U87-MG cells were transfected with pARF or pE by GLL; after 48 h incubation, the cell viability was determined by CyQuant assay. The values shown were mean values ± SD of at least three experiments. *$p < 0.05$, **$p < 0.01$, student's*t* test, two tails, equal variance.

The marker was Color marker ultra-low range (Sigma C6210).

For beta-actin detection, the same samples were resolved on a 12% Tris-HCl/SDS –polyacrylamide gel electrophoresis (Bio-Rad, Hercules, CA) and probed with Rabbit beta-actin antibody (1:1000 dilution in 5% fat free milk, Cell Signaling Technology, Danvers, MA), and horseradish peroxidase labeled anti-rabbit antibody was used as secondary antibody

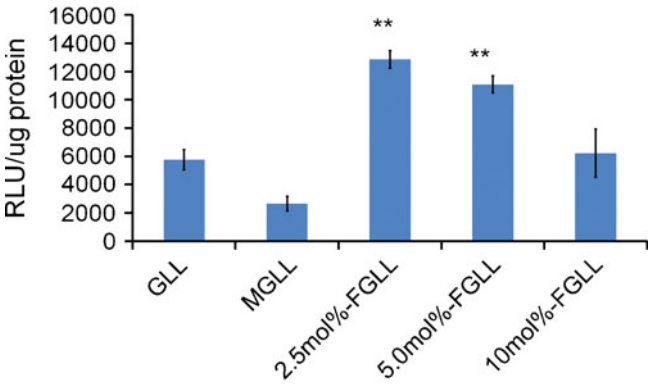

Fig. 5 Luciferase gene (PLC0888, pLUC) transfection on U87-MG cells by targeted formulations GLL means plasmid complex and stayed at 4°C overnight before transfection; MGLL was 5 mol% MPEG2000-DOPE added into GL89/LXS formulation, incubated 1 h at 37°C, then mixed with DNA, and stayed at 4°C overnight before transfection; 2.5 mol% -FGLL, 5 mol% -FGLL and 10 mol% -FGLL means FGF2-PEG-GL89/LXS by post-insertion method, the proper quantity of LXS was switched out for FGF2-PEG-DSPE. For each formulation, 0.2 μg DNA/0.2 ml/well, triplicate in 24-well plate for tansfection was used. One-way ANOVA analysis with multicomparison. $P < 0.0001$ between groups. **$p < 0.01$ when compared with GLL or MGLL groups.

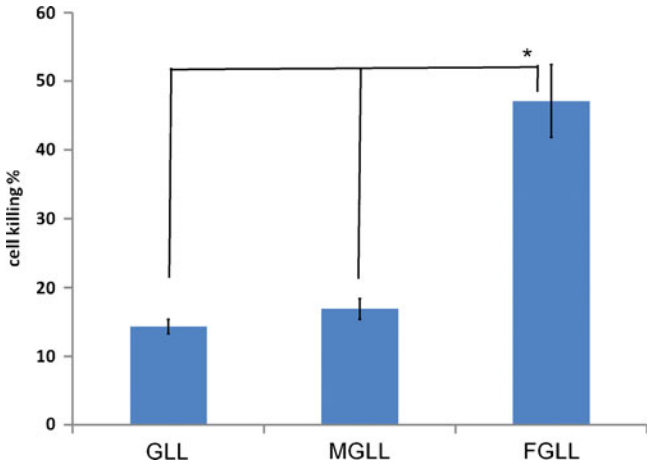

Fig. 6 *In vitro* pARF transfection in U87-MG cells GLL, MGLL and FGLL were ARF-TAT complex, with dialysis. The MPEG-PE or FGF2-PEG-DSPE mole percentage was 5 mol% of total lipids. 0.3 μg DNA in 0.2 ml serum-free media per well was used for transfection($n = 3$). *$p < 0.01$, FGLL *vs* GLL; * $p < 0.01$, FGLL *vs* MGLL according to One-Way ANOVA, with Turkey HD test.

(1:5000 dilution in 5% fat free milk, Cell Signaling Technology, Danvers, MA). The marker was Precision Plus Protein Kaleidoscope standards (Bio-Rad, Hercules, CA). The ECL Western Blotting Analysis System (GE Healthcare, UK) was used to detect immune-reactive proteins. All the Western blots were repeated at least three times.

TdT-Mediated dUTP Nick End Labeling (TUNEL) Assay

The fixed tumors were sectioned in 6–8 μm sections. The sections were performed with TUNEL staining according to the manufacturer's instructions. After staining, the slides were mounted individually using Vectashield® mounting medium with DAPI (Vector Laboratories, Inc. Burlingame, CA). Mounted slides were studied with a Zeiss Axiovert 200 M microscope fitted with a Zeiss AxioCam MRm camera (Carl Zeiss, Jena, Germany) under fluorescence using a FITC (fluorescein isothiocyanate) filter and a DAPI filter.

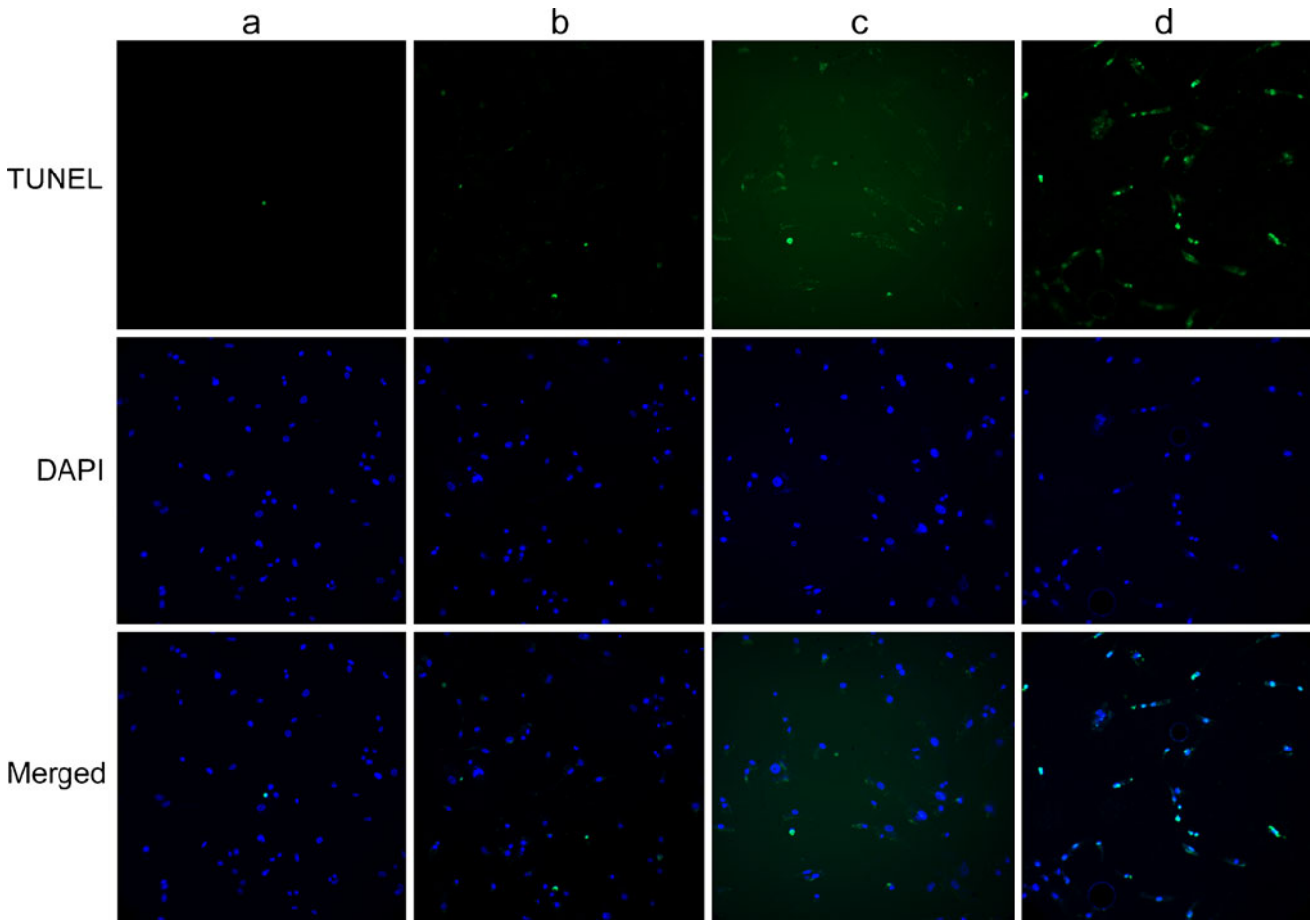

Fig. 7 Detection of apoptotic cells by TUNEL staining in U87-MG cells. Column a—no treatment cells; Column b—pE-GLL-transfected cells; Column c—pARF-GLL-transfected cells; Column d—pARF-FGLL-treated cells.

RESULTS

Conjugation of FGF2 with PDP-PEG-DSPE

The pyridyl thiol group of PDP-PEG-DSPE reacts specifically at pH7–9 by exchange with sulfhydryl of FGF2 peptide, leaving a pyridin-2-thione group that can be followed up; maximum absorbtion occurs at 343 nm with an extinction coefficient of 8.08×10^3 M^{-1} cm^{-1} (33). The formed link includes a –S-S- bound (disulfide). The same amount of PDP-PEG-DSPE reduced with dithiothreitol (DTT) was considered as a complete reaction. The conjugation efficiency of FGF2 peptide with PDP-PEG-DSPE was 95.10%±3.44% compared to DTT reduction. The ^{1}HNMR verification of the conjugation is provided in supplemental data (Fig. S1).

Size and Zeta Potential of the Lipoplexes

Size and zeta-potential of plain and targeted lipid mixture were measured before and after complexation with plasmid. The complex formation led to a moderate increase in size and decrease in zeta-potential (Table I). Before complex formation, the size of GLL was 107.1 nm±14.6 nm, and 114.1 nm±11.0 nm for FGLL. Upon complex formation with plasmid, the size increased to 289.3 nm±34.8 nm and 232.6 nm±29.0 nm, respectively. The zeta-potential of lipid mixture before complex formation was 34.5 mV±2.6 mV for GLL, and 6.58 mV±1.96 mV for FGLL. After the complexation with plasmid, the zeta-potential decreased to 28.1 mV±1.6 Mv for DNA-GLL and 5.11 mV±1.49 mV for DNA-FGLL. The low positive charge of FGLL and DNA-FGLL was due to the hydrophilic polymer shielding.

Biological Activity of pARF

The pARF expression in U87-MG cells was verified by a Western blot (Fig. 3). The gene product containing HA-tag was detected by HA-probe monoclonal antibody, as seen in Fig. 1, the band was located between 9–10 KD, which was larger than the 7 kD expected molecular weight. This is likely a result of post-translational modifications of the peptide consistent with the projected protein size from the plasmid sequence.

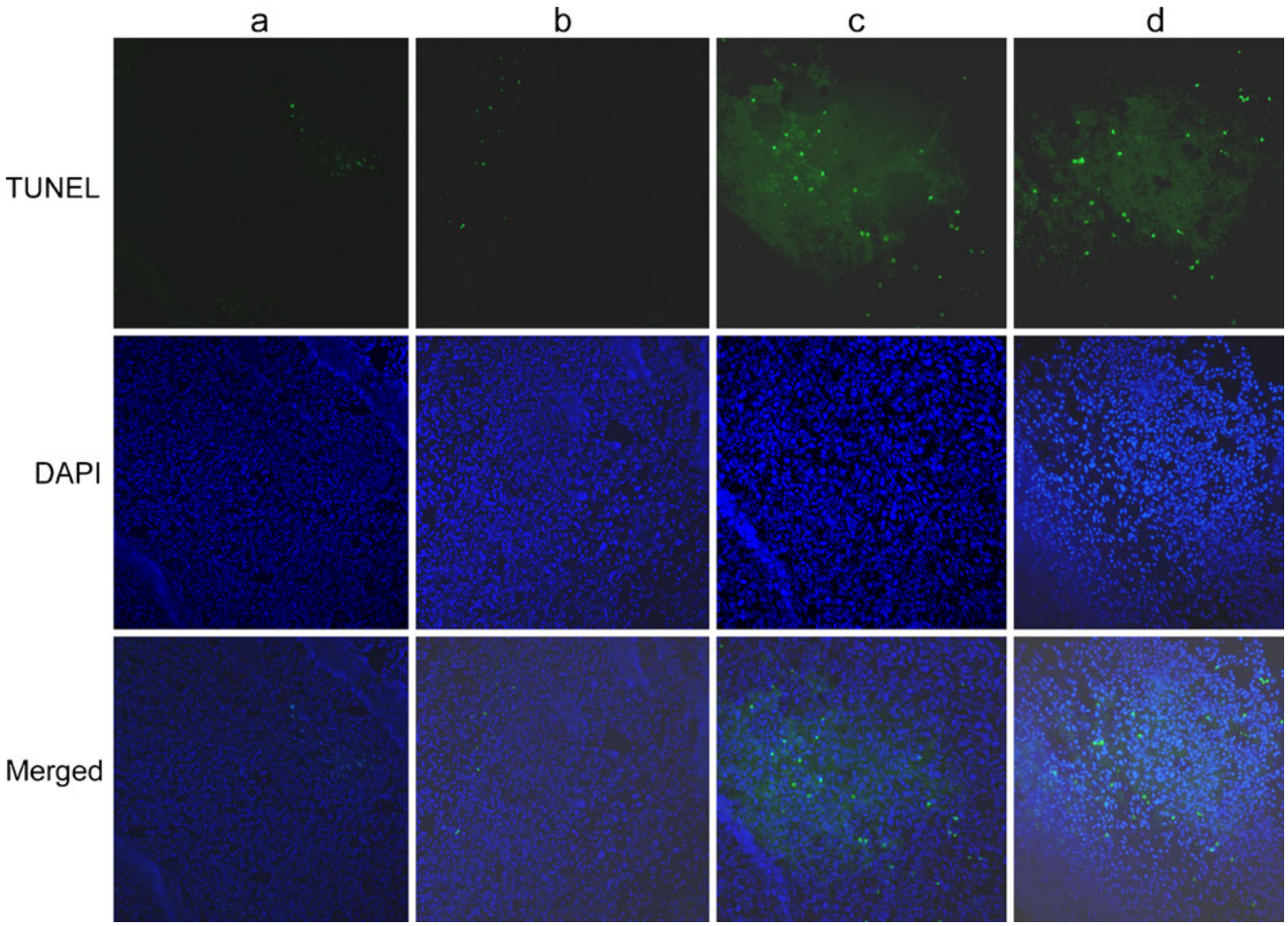

Fig. 8 TUNEL staining detection of apoptotic cells of xenograft U87-MG tumors. Column a—PBS; Column b—pE-GLL; Column c—pARF-GLL; Column d—pARF-FGLL.

An *in vitro* cytotoxicity study in which U87-MG cells were transfected with pARF plasmid demonstrated cellular toxicity percentage is between 15%–55% at the plasmid amount 0.2–1.0 μg/0.2 ml/well (Fig. 4).

Increased Transfection Efficiency by FGLL

The lipopeptide was prepared by conjugating FGF2-binding peptide with PDP-PEG2000-DSPE. The purified lipopeptide was incorporated into GLL-DNA complex to form the targeted lipoplex.

Luciferase gene (PLC0888) (34) transfected by GLL, MPEG-DSPE/GL89/LXS (MGLL) and FGF2-PEG-DSPE/GL89/LXS (FGLL) in U87-MG cells was performed for gene expression study (Fig. 5). According to one-way ANOVA analysis multicomparison, the p value of groups of luciferase expression was <0.0001, and there was a significant difference between 2.5 mol% FGLL or 5.0 mol% FGLL and GLL or MGLL ($p<0.01$) based on Tukey test. Specifically, when compared with GLL, the luciferase expression by FGLL increased 2.2-fold ($p<0.01$) at 2.5 mol%, 1.9-fold ($p<0.01$) at 5.0 mol% and 1.1-fold ($p>0.05$) at 10.0 mol%. When compared with 5.0 mol% MGLL, the luciferase expression by FGLL increased 4.8-fold ($p<0.01$) at 2.5 mol%, 4.2-fold ($p<0.01$) at 5.0 mol% and 2.4-fold ($p<0.01$) at 10.0 mol% (Fig. 5). Among the targeted groups with different amounts of FGF2-PEG-DSPE, 2.5 mol% and 5.0 mol% had a significantly higher expression than 10 mol% group ($p<0.01$). This result is likely due from a steric barrier effect of the pegylation (35).

The cytotoxicity of pARF transfected by GLL, 5.0 mol% MGLL and 5.0 mol% FGLL is shown in Fig. 6. According to one-way ANOVA analysis, the p between groups is under 0.0001. The Tukey HSD test showed that there is significant difference between the targeted group and non-targeted group (GLL or MGLL), $p<0.01$. The cell killing effect of pARF by FGLL was 3.3-fold higher than by GLL ($p<0.01$) and 2.8-fold higher than MGLL ($p<0.01$).

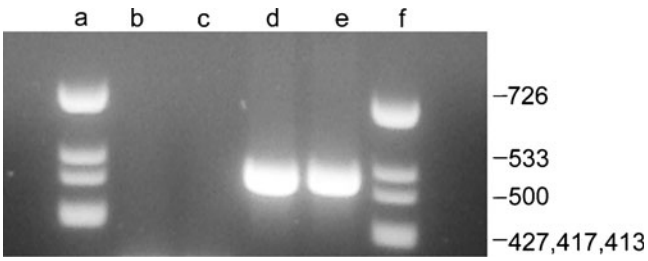

Fig. 9 Agarose gel electrophoresis of RT-PCR products of RNA extracted from pARF and pE-transfected tumors. Lane a, f—ΦX174 DNA/HinfI Markers (Promega, Madison, WI, USA); Lane b, c—pE-GLL treatment group tumors; Lane d—pARF-GLL treatment tumors; Lane e—pARF-FGLL-treated tumors.

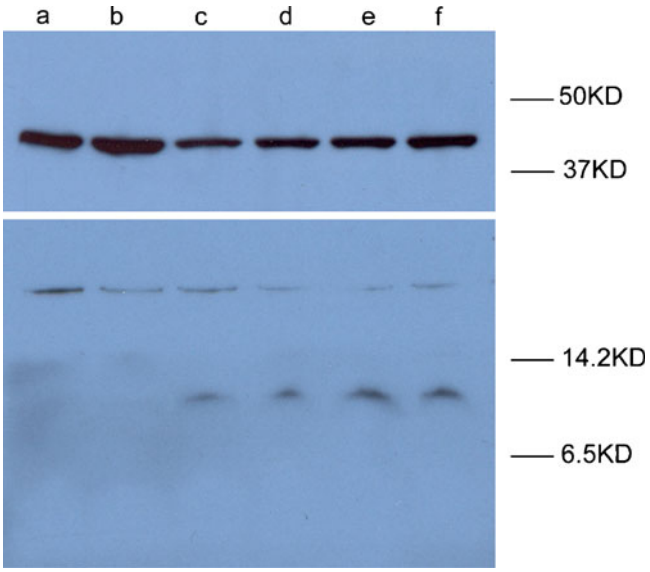

Fig. 10 Western blot detection of pARF *in vivo* expression. Lane a—tumor sample from PBS-treated mice; Lane b—tumor sample from pE-GLL-transfected mice; Lane c, d—tumor sample from pARF-GLL-transfected mice; Lane e, f—tumor sample from pARF-FGLL-transfected mice. The bands between 37KD and 50 KD were beta-actin. The bands between 6.5KD and 14.2KD were expected pARFproduct.

pARF Could Induce U87-MG Cell Apoptosis

U87-MG cell apoptosis was induced by pARF either delivered by GLL or 5.0 mol% FGLL, measured by TUNEL staining in cells and tumors (Figs. 7 and 8). More apoptotic positive cells were observed in the cells or tumor sections transfected by FGLL than by non-targeted GLL. This result verified that pARF could induce cell apoptosis by p14ARF-MDM2-P53 pathway (9,10).

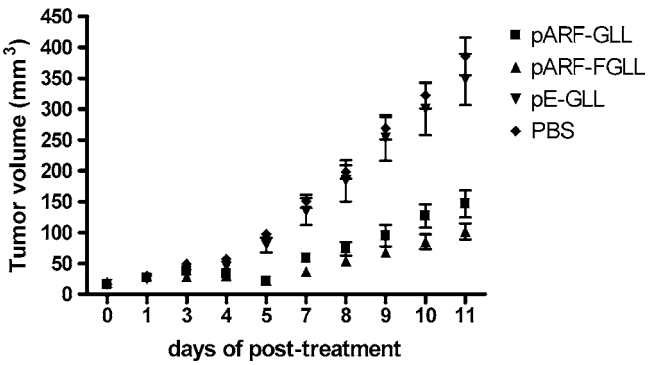

Fig. 11 pARF-FGLL complex suppress growth of subcutaneous human U87-MG cancer xenografts. Subcutaneous U87-MG tumor-bearing mice were divided into four groups (6 animals/group), and plasmid 50 μg/150 μl/mice injected twice via tail vein at the 4th day and the 11th day after the tumor cells implanted. Day 0 in X-axis means the 4th day following cell injection. PBS (diamond), pE-GLL (square), pARF-GLL (triangle) and pARF-FGLL (star). Tumors were measured using calipers. Each time point represents the mean tumor volume for each group (mean ± SEM, $n=6$).

Table II Tumor Volume and Weight Inhibition Percentage of pARF-FGLL

	PBS as control		pE-GLL as control	
	Volume inhibition% ± SEM	weight inhibition% ± SEM	Volume inhibition% ± SEM	weight inhibition% ± SEM
pARF-GLL	61.94 ± 11.25	61.81 ± 8.36	57.84 ± 12.47	57.42 ± 9.32
pARF-FGLL	73.48 ± 5.49*[a]	74.37 ± 4.25* [a]	70.62 ± 6.08* [b]	71.43 ± 4.73* [b]

One-way ANOVA analysis, multicomparison, * [a] $p < 0.05$, compared to PBS group, $n = 6$; * [b] $p < 0.05$, compared to pE-GLL group, $n = 6$

pARF was Expressed in Tumors following Systemic Administration of the Lipoplex

Since the expressed transgene protein is cytotoxic, we conducted a short-term experiment in which the gene expression was measured 24 h after gene delivery. Amplification of RNA by reverse transcription-PCR (RT-PCR) from tumors transfected with pARF-GLL (FGF2) and pE -GLL was analyzed by 2% agarose gel. pARF treatment tumors produced the expected band at 522 base pair (bp) (Fig. 9). Control samples that underwent the same RT-PCR protocol but without reverse transcriptase activation did not yield a product (data not shown).

In vivo gene expression of pARF delivered by GLL and FGLL was examined by Western blot. As shown in Fig. 10, pARF-transfected tumors had bands with size 9–10 KD, which was same as those from pARF in transfected cell lysate (Fig. 3). The bands observed between 14 KD and 37 KD were believed to be non-specific protein in mouse which could bind with anti-HA antibody but not existed in cells.

In Vivo Anti-Tumor Efficacy of pARF-FGLL Complex

The antitumor effect of pARF-FGLL complex was assessed in female nude/nude mice bearing subcutaneous U87-MG tumors with two doses. The tumor growth curve is shown in Fig. 11. According to one-way ANOVA analysis, the p value of groups on tumor volume change *versus* treatment time was 0.027, but not significant between groups. For tumor volume inhibition, the p value was 0.007, and there was significance between targeted treatment group and PBS or pE group according to Tukey HSD test and not significant between other groups. For tumor weight inhibition, the p value was 0.007, and there was significance between targeted treatment group and PBS or pE group according to Tukey HSD test and not significant between other groups (Table II). There was no significant difference in body weight of mice in all groups (data not shown).

The mice blood chemistry results are shown in Table III. The majority of the parameters were within the normal ranges. The total bilium values were higher than the reference. Since all the other liver parameters were in the normal range, and the blood sample was partially hemolyzed due to the mishandling, the total bilium was falsely increased by the hemolysis of the blood in this case.

DISCUSSION

This report illustrates the ability of targeted and non-targeted nanoparticles to deliver a functionally expressed gene cassette. The findings indicate that several vector features require attention in the design and implication. Current gene delivery vectors are often limited in their ability to reach the tumor, and if they reach their target, the intratumoral distribution can be severely limited. There may be other distribution factors such as intracellular transport also limiting activity. For expressed transgenes coding for intracel-

Table III Blood Chemistry of Nude Mice Bearing U87-MG Tumors at 24 h After DNA-Lipoplex Administration

TEST	Unit	50 μg DNA-200 μg GLL, iv.	Reference ranges[a]
Alanine aminotransferase (ALT)	U/L	25	51.3 ± 18.76
Aspartate aminotransferase (AST)	U/L	93	119.36 ± 95.49
Albumin (ALB)	g/dL	3	3.42 ± 0.38
BUN	mg/dL	21	18.52 ± 4.3
Glucose (GLU)	mg/dL	195	191.43 ± 30.51
Total protein (TPROT)	g/dL	5.8	5.74 ± 0.54
Calcium (CA)	mg/dL	10.8	10.71 ± 0.61
Inorganic phosphorus (PHOS)	mg/dL	9.7	10.41 ± 2.07
Cholesterol (CHOL)	mg/dL	107	134.28 ± 31.38
Total bilirubin (TBILI)	mg/dL	0.5	0.26 ± 0.08

[a] Reference ranges came from Charles River Laboratories International, Inc.

lular proteins, their biological activity is often restrained within the transfected cells or a few cells nearby via the bystander effect (36). On the other hand, the often-reported leaky vascular of tumors and many murine xenograft models can lead to nanoparticle accumulation via enhanced permeability and retention (EPR) effect (37). Thus, a targeting ligand might not be required, and the nature of the particle size, charge, and shape may be a larger driving force for tumor accumulation. For targeted particles, an additional concern is the requirement for the targeting ligand to reach the tumor cell surface. Many ligands occur on the tumor surface and not the vascular bed and depend on the EPR for initial accumulation. The judicial selection of an approach where the target is up-regulated in the tumor vascular bed and tumor cells is an attractive method of further increasing particle accumulation (*e.g.*, FGF receptor).

To address these limitations, a gene delivery paradigm was developed with several facets, including plasmid design and vector optimization. First, to increase the number of cells impacted, a transgene coding for a novel fusion protein was created. This fusion protein contained a domain that had been previously demonstrated to increase cell killing with an *in vitro* model (22). As previously demonstrated, three important domains were required: the ability of the protein to be secreted from the transfected cell (alkaline phosphatase domain), to enter adjacent cells (HIV TAT domain), and to elicit cytotoxicity (ARF14). It was demonstrated that the plasmid construct could lead to cytotoxcity, and this effect was correlated to expression levels. The current plasmid could be expressed in several cell types, leading to adverse effects. Optimization of the plasmid in terms of tissue-specific promoters could lead to a greater therapeutic window.

The gene delivery system was a novel set of surface-active agents with demonstrated ability to function *in vivo* (38,39). The cationic lipid Genzyme Lipid-89 in combination with helper lipids created a vector resistant to serum inactivation and limited cellular toxicity. To improve the *in vivo* transfection activity, a targeting moiety was incorporated. Recently, the importance and mechanisms of targeting nanoparticles *in vivo* have been updated. A current theory has the importance of the ligand more involved in either retaining the particle within a tissue or improving the intratumor/cellular distribution (40) instead of increasing the bulk tumor concentration. The selection of the targeting ligand was of some importance. FGF has two potential advantages: tumor cells have a high abundance of the receptor, and the new capillary endothelial cells allow nourishment to reach the tumor; in addition, the particle can lead to escape from the leaky vascular bed and accumulation. In this report, the actual accumulation of the particles was not measured, but tumor transgene expression and cytotoxicity effect were determined. It should be pointed out that expression and resulting effect could arise from expression in the vascular bed, tumor cells or other cells in the local tumor environment (tumor infiltrating macrophages, stromal cells *etc.*). Also, in other experiments with similar particles, expression occurred in other tissues (e.g., lung; data not shown). Thus, the overall biological effect could result from local expression and peptide transport from other tissues. From the data, it was clear that both the targeted and non-targeted particles lead to expression in the target area. The addition of the targeting ligand (5 mol% of total lipid) leads to greater amounts of the expressed protein in the tumor.

The overall effect on tumor growth is affected by several factors. If the fusion peptide functions as designed, there would be direct impact on tumor cells and potentially the nourishing vascular bed. We expect EPR to be the driving force for tumor accumulation, and the targeting approach to increase vascular effects and tumor nanoparticle retention. The vector composed of a cationic lipid could also result in some of the added toxicity (41). Also, the administration of plasmid DNA can stimulate the immune system (42), leading to an antitumor effect.

In summary, we have reported a new composite nanoparticle, with design characteristics relating to the expressed protein and delivery vector. The ability of the cationic nanoparticle to express the transgene of interest was demonstrated using both *in vitro* and *in vivo* models. The results indicated that many factors need to be considered in the development of gene vectors for cancer, but the composite approach is one promising paradigm.

ACKNOWLEDGMENTS

Thanks to Carlos Castro and Nam Nguyen for the technician work, to Dr. Yuanqing Lu for mice tail vein injection, and Jim Rocca for help on ^{1}H-NMR analysis. In addition, the authors would like to thank the ICBR Proteomics Lab, University of Florida for FGF2 peptide synthesis. This work was supported by the Bankhead-Coley State of Florida Biomedical Fund and Roche Post Doctoral Fellowship Program.

REFERENCES

1. Edelstein ML, Abedi MR, Wixon J, Edelstein RM. Gene therapy clinical trials worldwide 1989–2004-an overview. J Gene Med. 2004;6:597–602.
2. Gomez-Navarro J, Curiel DT. Conditionally replicative adenoviral vectors for cancer gene therapy. Lancet Oncol. 2000;1:148–58.
3. Clark PR, Hersh EM. Cationic lipid-mediated gene transfer: current concepts. Curr Opin Mol Ther. 1999;1:158–76.
4. Sosnowski BA, Gu DL, D'Andrea M, Doukas J, Pierce GF. FGF2-targeted adenoviral vectors for systemic and local disease. Curr Opin Mol Ther. 1999;1:573–9.

5. Chandler LA, Sosnowski BA, Greenlees L, Aukerman SL, Baird A, Pierce GF. Prevalent expression of fibroblast growth factor (FGF) receptors and FGF2 in human tumor cell lines. Int J Cancer. 1999;81:451–8.
6. Kobayashi H, Sakahara H, Hosono M, Shirato M, Konishi J, Takahashi JA, *et al.* Scintigraphic detection of xenografted tumors producing human basic fibroblast growth factor. Cancer Immunol Immunother. 1993;37(5):281–5.
7. Kono K, Ueba T, Takahashi JA, Murai N, Hashimoto N, Myoumoto A, *et al. In vitro* growth suppression of human glioma cells by a 16-mer oligopeptide: a potential new treatment modality for malignant glioma. J Neurooncol. 2003;63(2):163–71.
8. Trudel C, Faure-Desire V, Florkiewicz RZ, Baird A. Translocation of FGF2 to the cell surface without release into conditioned media. J Cell Physiol. 2000;185(2):260–8.
9. Stan AC, Nemati MN, Pietsch T, Walter GF, Dietz H. *In vivo* inhibition of angiogenesis and growth of the human U-87 malignant glial tumor by treatment with an antibody against basic fibroblast growth factor. J Neurosurg. 1995;82:1044–52.
10. Murphy PR, Sato Y, Knee RS. Phosphorothioate antisense oligonucleotides against basic fibroblast growth factor inhibit anchorage-dependent and anchorage-independent growth of a malignant glioblastoma cell line. Mol Endocrinol. 1992;6(6):877–84.
11. Basilico C, Moscatelli D. The FGF family of growth-factors and oncogenes. Adv Cancer Res. 1992;59:115–65.
12. Kurokawa T, Sasada R, Iwane M, Igarashi K. Cloning and expression of cDNA encoding human basic fibroblast growth factor. FEBS Lett. 1987;213:189–94.
13. Maruta F, Parker AL, Fisher KD, Hallissey MT, Ismail T, Rowlands DC, *et al.* Identification of FGF receptor-binding peptides for cancer gene therapy. Cancer Gene Ther. 2002;9(6):543–52.
14. Rao GA, Tsai R, Roura D, Hughes JA. Evaluation of the transfection property of a peptide ligand for the fibroblast growth factor receptor as part of PEGylated polyethylenimine polyplex. J Drug Target. 2008;16(1):79–89.
15. Izard JW, Kendall DA. Signal peptides: exquisitely designed transport promoters. Mol Microbiol. 1994;13:765–73.
16. Vives E, Richard JP, Rispa C, Lebleu B. TAT peptide internalization: seeking the mechanism of entry. Curr Protein Pept Sci. 2003;4:125–32.
17. Schwarze SR, Ho A, Vocero-Akbani A, Dowdy SF. *In vivo* protein transduction: delivery of a biologically active prote*in into* the mouse. Science. 1999;285:1569–72.
18. Richard JP, Melikov K, Vives E, Ramos C, Verbeure B, Gait MJ, *et al.* Cell-penetrating peptides. A reevaluation of the mechanism of cellular uptake. J Biol Chem. 2003;278:585–90.
19. Deb SP. Cell cycle regulatory functions of the human oncoprotein MDM2. Mol Cancer Res. 2003;1:1009–16.
20. Buschmann T, Minamoto T, Wagle N, Fuchs SY, Adler V, Mai M, *et al.* Analysis of JNK, Mdm2 and p14(ARF) contribution to the regulation of mutant p53 stability. J Mol Biol. 2000;295 (4):1009–21.
21. p19ARF links the tumour suppressor p53 to Ras. Palmero I, Pantoja C, Serrano M. Nature. 1998;395(6698):125–6.
22. Jarajapu YP, Baltunis J, Knot HJ, Sullivan SM. Biological evaluation of penetration domain and killing domain peptides. J Gene Med. 2005;7:908–17.
23. Baskar JF, Smith PP, Nilaver G, Jupp RA, Hoffmann S, Peffer NJ, *et al.* The enhancer domain of the human cytomegalovirus major immediate-early promoter determines cell type-specific expression in transgenic mice. J Virol. 1996;70(5):3207–14.
24. Robert-Guroff M, Popovic M, Gartner S, Markham P, Gallo RC, Reitz MS. Structure and expression of tat-, rev-, and nef-specific transcripts of human immunodeficiency virus type 1 in infected lymphocytes and macrophages. J Virol. 1990;64:3391–8.
25. Gyongyossy-Issa MI, Muller W, Devine DV. The covalent coupling of Arg-Gly-Asp-containing peptides to liposomes: purification and biochemical function of the lipopeptide. Arch Biochem Biophys. 1998;353:101–8.
26. Sosnowski BA, Gonzalez AM, Chandler LA, Buechler YJ, Pierce GF, Baird A. Targeting DNA to cells with basic fibroblast growth factor (FGF2). J Biol Chem. 1996;271:33647–53.
27. Li D, Yu H, Huang H, Shen F, Wu X, Li J, *et al.* FGF receptor-mediated gene delivery using ligands coupled to polyethylenimine. J Biomater Appl. 2007;22:163–80.
28. Driessen WH, Fujii N, Tamamura H, Sullivan SM. Development of peptide-targeted lipoplexes to CXCR4-expressing rat glioma cells and rat proliferating endothelial cells. Mol Ther. 2008;16:516–24.
29. Li S, Driessen WH, Sullivan SM and Jiang H. Bioluminescence tomography based on phantoms with different concentrations of bioluminescent cancer cells. J Opt A: Pure Appl. 2006;743–6.
30. Peeters L, Sanders NN, Jones A, Demeester J, De Smedt SC. Post-pegylated lipoplexes are promising vehicles for gene delivery in RPE cells. J Contr Release. 2007;121:207–17.
31. Krishnadas A, Rubinstein I, Onyüksel H. Sterically stabilized phospholipid mixed micelles: *in vitro* evaluation as a novel carrier for water-insoluble drugs. Pharm Res. 2003;20:297–302.
32. Tomayko MM, Reynolds CP. Determination of subcutaneous tumor size in athymic (nude) mice. Cancer Chemother Pharmacol. 1989;24(3):148–54.
33. Struchbury T, Shipton M, Norris R, Malthouse JPG, Brocklehurst K. Reporter group delivery system with both absolute and select ive specificity for thiol groups and an improved fluorescent probe containing the 7-nitrobenzo-2-oxa-1.3-diazole moiety. Biochem J. 1975;151:417–32.
34. Li S, MacLaughlin FC, Fewell JG, Li Y, Mehta V, French MF, *et al.* Increased levels and duration of expression in muscle by co-expression of a transactivator using plasmid systems. Gene Ther. 1999;6:2005–11.
35. Song LY, Ahkong QF, Rong Q, Wang Z, Ansell S, Hope MJ, *et al.* Characterization of the inhibitory effect of PEG-lipid conjugates on the intracellular delivery of plasmid and antisense DNA mediated by cationic lipid liposomes. Biochim Biophys Acta. 2002;1558(1):1–13.
36. Cao L, Si J, Wang W, Zhao X, Yuan X, Zhu H, *et al.* Intracellular localization and sustained prodrug cell killing activity of TAT-HSVTK fusion protein in hepatocelullar carcinoma cells. Mol Cells. 2006;21(1):104–11.
37. Fang J, Nakamura H, Maeda H. The EPR effect: Unique features of tumor blood vessels for drug delivery, factors involved, and limitations and augmentation of the effect. Adv Drug Deliv Rev. 2010 May 2. [Epub ahead of print].
38. Shaw LC, Pan H, Afzal A, Li Calzi S, Spoerri PE, Sullivan SM, *et al.* Proliferating endothelial cell-specific expression of IGF-I receptor ribozyme inhibits retinal neovascularization. Gene Ther. 2006;13:752–60.
39. Kielczewski JL, Jarajapu YP, McFarland EL, Cai J, Afzal A, Li Calzi S, *et al.* Insulin-like growth factor binding protein-3 mediates vascular repair by enhancing nitric oxide generation. Circ Res. 2009;105(9):897–905.
40. Choi CH, Alabi CA, Webster P, Davis ME. Mechanism of active targeting in solid tumors with transferrin-containing gold nanoparticles. Proc Natl Acad Sci USA. 2010;107(3):1235–40.
41. Niu G, Castro CH, Nguyen N, Sullivan SM, Hughes JA. *In vitro* cytotoxic activity of cationic paclitaxel nanoparticles on MDR-3T3 cells. J Drug Target. 2010;18(6):468–76.
42. Rudginsky S, Siders W, Ingram L, Marshall J, Scheule R, Kaplan J. Antitumor activity of cationic lipid complexed with immunostimulatory DNA. Mol Ther. 2001;4(4):347–55.